Internal dark matter structure of the most massive galaxy clusters — **Source link** ⧉

Amandine M. C. Le Brun, Monique Arnaud, Gabriel W. Pratt, Romain Teyssier

Related papers:

- The universal galaxy cluster pressure profile from a representative sample of nearby systems (REXCESS) and the Y-SZ-M-500 relation

- Planck 2013 results. XXIX. The Planck catalogue of Sunyaev-Zeldovich sources

- Galaxy clusters discovered via the Sunyaev-Zel'dovich effect in the 2500-square-degree SPT-SZ survey

- The cool-core state of Planck SZ-selected clusters versus X-ray-selected samples: evidence for cool-core bias

- Planck 2015 results. XXVII. The Second Planck Catalogue of Sunyaev-Zeldovich Sources

Share this paper: 𝕗 𝕏 in ✉

View more about this paper here: https://typeset.io/papers/internal-dark-matter-structure-of-the-most-massive-galaxy-2gh2twbatv

Year: 2018

Internal dark matter structure of the most massive galaxy clusters

Le Brun, A M C ; Arnaud, M ; Pratt, G W ; Teyssier, R

Abstract: We investigate the evolution of the dark matter density profiles of the most massive galaxy clusters in the Universe. Using a 'zoom-in' procedure on a large suite of cosmological simulations of total comoving volume of 3 $(h − 1 \, \mathrm{Gpc})^3$, we study the 25 most massive clusters in four redshift slices from z 1 to the present. The minimum mass is $M500 > 5.5 \times 10^{14} \, M$ at z = 1. Each system has more than two million particles within r500. Once scaled to the critical density at each redshift, the dark matter profiles within r500 are strikingly similar from z 1 to the present day, exhibiting a low dispersion of 0.15 dex, and showing little evolution with redshift in the radial logarithmic slope and scatter. They have the running power-law shape typical of the Navarro–Frenk–White type profiles, and their inner structure, resolved to 3.8 h−1 comoving kpc at z = 1, shows no signs of converging to an asymptotic slope. Our results suggest that this type of profile is already in place at z > 1 in the highest-mass haloes in the Universe, and that it remains exceptionally robust to merging activity.

Internal dark matter structure of the most massive galaxy clusters

A. M. C. Le Brun,[1,2]★ M. Arnaud,[1,2] G. W. Pratt[1,2] and R. Teyssier[3]

[1]*IRFU, CEA, Université Paris-Saclay, F-91191 Gif-sur-Yvette, France*
[2]*Université Paris Diderot, AIM, Sorbonne Paris Cité, CEA, CNRS, F-91191 Gif-sur-Yvette, France*
[3]*Institute for Computational Science, University of Zürich, CH-8057 Zürich, Switzerland*

ABSTRACT

We investigate the evolution of the dark matter density profiles of the most massive galaxy clusters in the Universe. Using a 'zoom-in' procedure on a large suite of cosmological simulations of total comoving volume of $3\,(h^{-1}\,\mathrm{Gpc})^3$, we study the 25 most massive clusters in four redshift slices from $z \sim 1$ to the present. The minimum mass is $M_{500} > 5.5 \times 10^{14}\,\mathrm{M_\odot}$ at $z = 1$. Each system has more than two million particles within r_{500}. Once scaled to the critical density at each redshift, the dark matter profiles within r_{500} are strikingly similar from $z \sim 1$ to the present day, exhibiting a low dispersion of 0.15 dex, and showing little evolution with redshift in the radial logarithmic slope and scatter. They have the running power-law shape typical of the Navarro–Frenk–White type profiles, and their inner structure, resolved to $3.8\,h^{-1}$ comoving kpc at $z = 1$, shows no signs of converging to an asymptotic slope. Our results suggest that this type of profile is already in place at $z > 1$ in the highest-mass haloes in the Universe, and that it remains exceptionally robust to merging activity.

Key words: galaxies: clusters: general – galaxies: evolution – galaxies: structure – large-scale structure of Universe – cosmology: miscellaneous.

1 INTRODUCTION

While the theoretical paradigm for the formation and evolution of large-scale structure in a dark-matter-dominated universe was described over 35 yr ago (e.g. Peebles 1980), it is only recently that observations have definitively established the conceptual framework within which this process takes place (e.g. Hinshaw et al. 2013; Planck Collaboration XVI 2014; Planck Collaboration XIII 2016). Today, the hierarchical collapse of dark matter into clumps or 'haloes' in the dark-energy dominated cold dark matter (ΛCDM) model is a cornerstone of our understanding of the formation of galaxies, galaxy groups and clusters.

The most massive galaxy clusters, defined here as those with $M_{500} > 5 \times 10^{14}\,\mathrm{M_\odot}$, occupy a unique position in the cosmic hierarchy.[1] They are dark matter-dominated, except in the very centre. Their deep potential wells ensure that gravity is the dominant mechanism driving their evolution, leaving their observed properties least affected by the complicated non-gravitational processes linked to galaxy formation (e.g. Cui, Borgani & Murante 2014; Martizzi et al. 2014; Velliscig et al. 2014). They are observable up to high redshift, and complementary techniques can be used to probe their internal structure and measure their scaling properties. For these

reasons, they are ideal objects with which to test theories of structure formation.

The advent of Sunyaev–Zel'dovich (SZ) surveys has led to an explosion in the number of known high-redshift clusters (Hasselfield et al. 2013; Planck Collaboration XXIX 2014; Bleem et al. 2015; Planck Collaboration XXVII 2016). Many of these are high mass, and recent results have demonstrated the feasibility of obtaining high-quality structural and scaling information from these objects (e.g. Schrabback et al. 2016; Bartalucci et al. 2017). In particular, X-ray observations of these bright systems can probe the $[0.05–1]\,r_{500}$ radial range with relative ease (Bartalucci et al. 2017).

Numerical simulations of structure formation in the ΛCDM cosmology make a number of observationally-testable predictions, such as for instance the existence of a quasi-universal, cuspy, dark matter density profile (e.g. Navarro, Frenk & White 1997). However, existing simulations are poorly adapted to the specific case of high-mass, high redshift systems, as often their resolution is inadequate to match the observations, and/or the number of simulated objects is limited. The present study expands upon the existing body of work on the structure of massive dark matter haloes (e.g. Tasitsiomi et al. 2004; Gao et al. 2012; Wu et al. 2013) by increasing the spatial or mass resolution and the number of objects. More fundamentally, we simulate the most massive galaxy clusters at $z > 0$, and not just the progenitors of the $z = 0$ systems. We find that the dark matter profiles of these systems are strikingly similar from $z \sim 1$ to the present day, and exhibit a low dispersion (0.15 dex within r_{500}).

★ E-mail: amandine.le-brun@cea.fr
[1] see below for definition of M_{500}

This Letter is organized as follows. We briefly introduce the new suite of simulations in Section 2, discuss the structural evolution from $z = 1$ to the present day in Section 3, and discuss our results and conclude in Section 4. Throughout this Letter, M_Δ is the mass within radius r_Δ, the radius within which the mean mass density is Δ times the critical density at the cluster redshift.

2 SIMULATIONS AND DATA PROCESSING

We tailored our simulations to produce a moderately large sample ($\sim$50) of massive ($M_{500} \gtrsim 5 \times 10^{14}\,M_\odot$) objects at $z \sim 1$, comparable to current SZ observational surveys in terms of mass, and with a sample size sufficient to derive robust statistical conclusions. The deepest current observational survey follow-up data sets resolve the inner structure at the tens of kiloparsec scale (e.g. Bartalucci et al. 2017). A simulation reproducing these characteristics would require a $\gtrsim 1\,\mathrm{Gpc}^3$ volume to be simulated at high resolution. This being impossible given current computational resources, we adopted a strategy in which the total volume was split into three periodic boxes of $1\,h^{-1}$ comoving Gpc on a side containing 2048^3 dark matter particles, and used the 'zoom-in' technique to further refine individual systems from these parent large box simulations.

The cosmological parameters were taken from Planck Collaboration XIII (2016) with $\{\Omega_m, \Omega_b, \Omega_\Lambda, \sigma_8, n_s, h\} = \{0.3156, 0.0492, 0.6844, 0.831, 0.9645, 0.6727\}$. The initial conditions were generated at a starting redshift of $z = 100$ using MUSIC (Hahn & Abel 2011) in second-order Lagrangian perturbation theory mode and a transfer function computed with the 2015 January version of the Boltzmann code CAMB[2] (Lewis, Challinor & Lasenby 2000). The simulations were carried out with the Eulerian adaptive mesh refinement (AMR) code RAMSES (Teyssier 2002) with an initial level of refinement $\ell = 11$ (2048^3). Six additional levels of refinement were significantly triggered during the run ($\ell_{max} = 17$). This corresponds to a spatial resolution of $\sim 15\,h^{-1}$ comoving kpc (ckpc; computed as $r_{min} = 2 \times L_{box}/2^{\ell_{max}}$ i.e. corresponding to two times the sidelength of the AMR cells of level ℓ_{max}). This estimate of the spatial resolution is very conservative. A quasi-Lagrangian refinement strategy was used (i.e. the cells were split if they contained more than eight particles). Haloes were identified using PHEW, the on-the-fly halo finder implemented in RAMSES (Bleuler et al. 2015). Each halo was recentred using a shrinking sphere procedure (e.g. Power et al. 2003) and then spherical overdensity masses M_Δ were computed.

The 'zoom' initial conditions were also generated using MUSIC for a sphere of $8\,h^{-1}$ cMpc radius, at the selection redshift z_{sel} defined below, centred on the selected system. However, if the central halo was contaminated by low-resolution particles at more than the $\sim 10^{-3}$ level, the simulation was re-run using a sphere of $16\,h^{-1}$ cMpc radius instead. This only affects one system at $z_{sel} = 1$ system and one at $z_{sel} = 0.8$. We needed an effective resolution of 8192^3 (8K) particles (see Appendix A), resulting in a particle mass of $m_{cdm} = 1.59 \times 10^8\,h^{-1}\,M_\odot$. The main haloes thus contain at least $\sim$2 million particles within r_{500}. We used the same quasi-Lagrangian refinement strategy as for the large boxes, resulting in $\ell_{max} = 19$, corresponding to spatial resolutions of $\sim 3.8\,h^{-1}$ ckpc.

Here, we focus on the dark matter only (DMO) 'zooms' of the 25 most massive systems selected in four different redshift slices

Table 1. Main characteristics of the 25 most massive sample for each redshift slice.

Redshift slice	Min(M_{500}) ($10^{14}\mathrm{M}_\odot$)	Median(M_{500}) ($10^{14}\mathrm{M}_\odot$)	Max(M_{500}) ($10^{14}\mathrm{M}_\odot$)	f_{rel}
$z_{sel} = 1$	5.55	6.32	13.9	24 per cent
$z_{sel} = 0.8$	7.27	8.31	12.8	16 per cent
$z_{sel} = 0.6$	8.97	10.6	30.0	32 per cent
$z_{sel} = 0$	19.2	22.6	36.5	40 per cent
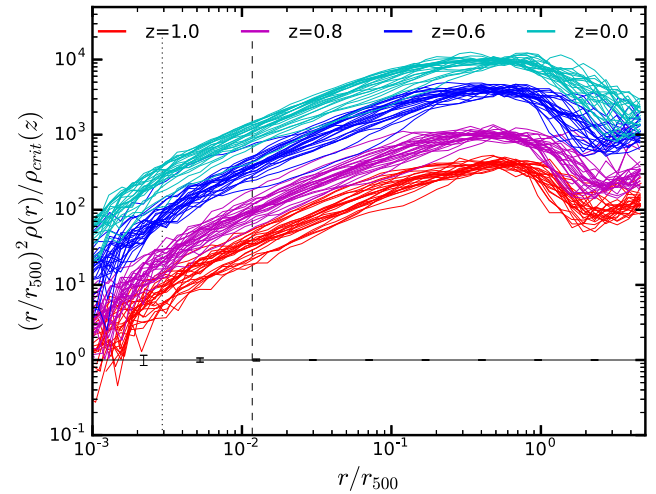
Figure 1. Spherical density profiles for each redshift slice. For clarity, the profiles of the $z_{sel} = 1, 0.8, 0.6$ and 0 systems have been shifted up by a factor of 2, 5, 20 and 50, respectively. The resolution limit at $z = 0$ is depicted as dashed and dotted vertical lines for the large boxes and the DMO zooms, respectively. The typical Poisson errors for every fifth data point are displayed as black error bars.

($z_{sel} = 1, 0.8, 0.6$ and 0^3). The main characteristics of the subsample at each z_{sel}, including the resulting minimum mass, are summarized in Table 1. The sample grows by nearly a factor of four in median mass between $z = 1$ and 0. The relaxed fraction f_{rel} is computed as the fraction of systems with $\Delta r \leq 0.04$ (Power, Knebe & Knollmann 2012), where Δr is the distance between the centre of mass within the Bryan & Norman (1998) virial radius r_{vir} and the centre of the shrinking sphere, in units of r_{vir}. A resolution study shows that the 8K zooms (i.e. the nominal resolution) are converged (in particular with the even-higher resolution 16K runs) over the whole resolved ($r \geq r_{min}^{8K}$) radial range (see Appendix A), and that an effective resolution of 8192^3 is the minimum required for this work.

Fig. 1 shows the density profiles computed using 50 evenly spaced logarithmic bins over the $10^{-3} \leq r/r_{500} \leq 5$ radial range with the PYMSES[4] PYTHON module. We use mass-weighted radii in this and subsequent figures. The resolution limits at $z = 0$ (the maximum value of r_{min}/r_{500}) are displayed as black dashed and dotted lines for the large boxes and the DMO zooms, respectively. Both limits are nearly redshift-independent as, with increasing redshift, the decrease in the minimum value of r_{500} is nearly compensated for by the

---

[2] http://camb.info/

[3] This redshift distribution has been chosen to match an observational sample at $z \gtrsim 0.5$ (Arnaud et al. in preparation; Bartalucci et al. 2017) as well as providing a 'local reference' for comparison with both observations and previous theoretical work.

[4] http://irfu.cea.fr/Projets/PYMSES/intro.html
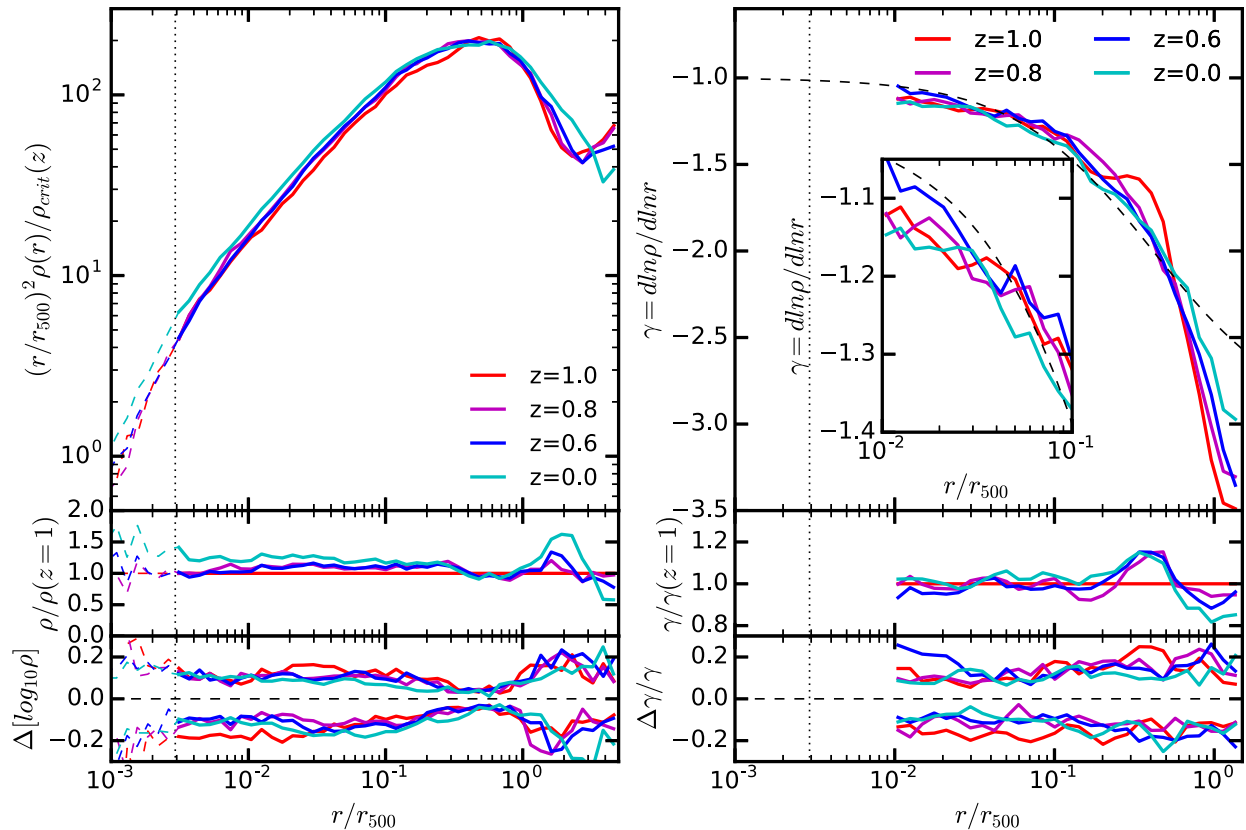
Figure 2. Median spherical density (top left-hand panel) and logarithmic slope (top right-hand panel) profiles for each redshift slice. The middle panels show the median profiles normalized by the median profile at $z_{sel} = 1$, whereas the bottom panels display the difference between the 16/84 percentiles and the median. In all panels, the resolution limit at $z = 0$ is depicted as a dotted line, and the profiles are plotted either as dashed thinner lines below that limit for the density or only from the eighth radial bin above that limit for the logarithmic slope where the Savitzky–Golay filter method is valid. The inset in the top right-hand panel is a zoom-in of the $0.01 \leq r/r_{500} \leq 0.1$ radial range.

increase of r_{min} given in comoving units. The 'zoom-in' procedure results in the gain of at least a factor of five in spatial resolution. Being smaller than the Poisson errors, the fluctuations are real and are likely due to the presence of substructures, and to oscillations resulting from the relaxation of the haloes.

Densities were normalized by the critical density of the Universe at the cluster redshift, and the radii by the corresponding r_{500}. This choice was motivated by the fact that the inner profiles are expected to evolve most self-similarly when rescaled in terms of the critical density (Diemer & Kravtsov 2014), and that the region $r/r_{500} \lesssim 1$ can be routinely probed by observations. We multiplied the scaled densities by $(r/r_{500})^2$ to reduce the dynamic range of the y-axis. To quantify the profile shapes, we computed the logarithmic slope $\gamma \equiv \mathrm{d} \ln \rho/\mathrm{d} \ln r$ from the smallest resolved radius [max (r_{min}/r_{500}) $\lesssim 0.003$], using the fourth-order Savitzky–Golay algorithm over the 15 nearest bins (Savitzky & Golay 1964). Excluding the seven innermost and outermost bins where the method is no longer valid, the logarithmic slope profiles cover the $0.01 \leq r/r_{500} \leq 1.35$ radial range.

3 STRUCTURAL EVOLUTION FROM $z = 1$

The left-hand panels of Fig. 2 show the median scaled density profiles of each redshift slice. In the standard self-similar model, we expect the density profiles to be identical, irrespective of the cluster redshift or any other characteristics. Hereafter, evolution refers to the evolution of the scaled profiles, i.e. additional evolution

in excess of the self-similar expectation. The mean density within r_{500} being proportional to $\rho_{crit}(z)$ by definition, scaled profiles may only differ by their shape in the region $r/r_{500} < 1$. Additionally, they are expected to cross around $r/r_{500} \sim 0.6$, the radius enclosing half of M_{500}, and thus their scatter to be minimal around that radius. Beyond r_{500}, a breaking of self-similarity could translate into evolution in both shape and overall normalization.

The scaled profiles display a barely noticeable evolution for $1 \geq z \geq 0.6$ over the whole radial range probed by the simulations. They change by never more than a factor of ~ 1.2 with decreasing redshift (see the middle panel). Conversely, they evolve a bit more (by up to a factor of ~ 1.5) both in the core ($r/r_{500} \lesssim 0.2$) and the outskirts ($r/r_{500} \gtrsim 1.5$) for $z \leq 0.6$. This is consistent with the 'stable clustering' hypothesis often used for computing the non-linear matter power spectrum (e.g. Peebles 1980). The former evolution corresponds to a slight increase of peakiness. The latter is most likely mostly due to their mass growth. The evolution in the outskirts corresponds to the transition between the one- and two-halo terms moving outwards as the haloes grow. It is thus especially noticeable as the median masses of the respective samples more than double from $M_{500} = 1.06 \times 10^{15} \, \mathrm{M}_\odot$ to $M_{500} = 2.26 \times 10^{15} \, \mathrm{M}_\odot$ between $z = 0.6$ and $z = 0$. Note that up to between 42 (between $z = 1$ and 0) and 83 per cent (between $z = 1$ and 0.8) of this mass growth could be due to pseudo-evolution (e.g. Diemer, More & Kravtsov 2013; Wu et al. 2013).

The scatter of the density profiles, as depicted in the bottom panel, is remarkably small over the redshift and radial ranges

($\lesssim 0.2\,\mathrm{dex}$). The scatter is less than 0.15 dex within r_{500}. In the outskirts, it is slightly larger than in the core and seems to increase mildly (by ~ 30 per cent) with redshift. Note that these trends need to be confirmed with the whole set of simulations as each redshift slice contains only 25 systems. The minimum around $r/r_{500} \sim 0.6$ is a consequence of the normalization of the profiles as mentioned above.

The high degree of self-similarity is confirmed when studying the profile shapes. The right-hand panels of Fig. 2 show the median logarithmic slope profiles of each redshift slice. They exhibit small amounts of both evolution (which never exceeds 20 per cent; see the middle panel) and dispersion ($\lesssim 0.2\,\mathrm{dex}$; see the bottom panel) over the whole redshift and radial range. Similarly to the density profiles, the evolution is more important in the very central regions ($r/r_{500} \lesssim 0.02$) and the outer regions ($r/r_{500} \gtrsim 0.6$). More unexpectedly, the slope of the profiles, displays noticeable evolution for all $z \leq 1$ and not just $z \leq 0.6$.

The scatter of the density slope displays nearly no evolution over the whole radial range and is similar in amplitude to that of the density profiles (except around $r/r_{500} \sim 0.6$, where the scatter of the density is minimum by construction). More importantly, the inner slope shows no signs of converging to an asymptotic value but is still consistent with a Navarro–Frenk–White (NFW) profile of typical concentration for massive galaxy clusters ($c_{200} = 3.5$) over the radial range in question (see the top right-hand panel and its inset; in agreement with the results of e.g. Navarro et al. 2004).

A first investigation of the origin of the scatter in the density profiles is illustrated by Fig. 3, which displays the M_{500}/M_{2500} ratio as a function of Δr. The most relaxed clusters ($\Delta r \leq 0.04$) tend to be more centrally concentrated, i.e. they have a smaller M_{500}/M_{2500} ratio ($M_{500}/M_{2500} \lesssim 4$). However, there is no clear correlation between both parameters in terms of Spearman's rank and null hypothesis probability, as listed in the legend of Fig. 3. In fact, the distribution is consistent with all systems having a similar M_{500}/M_{2500} ratio, irrespective of their relaxation state, but with a dispersion that increases with increasing Δr. Therefore, the scatter in the density profiles is connected only to the relaxation state of the galaxy cluster through the fact that relaxed clusters are mostly centrally concentrated, while unrelaxed objects span a larger variety of profile shapes, including very shallow profiles. Note that the entire simulation sample is required to reach a reliable conclusion on this point.

4 DISCUSSION AND CONCLUSION

We have focused in this work on the dark matter density profiles of the 25 most massive systems selected from DMO simulations in four redshift slices ($z_{\mathrm{sel}} = 1$, 0.8, 0.6 and 0). With a median mass of $M_{500} = 6.3 \times 10^{14}\,\mathrm{M}_{\odot}$ at $z = 1$, the sample is composed of the rarest objects, probing for the first time the extreme limits of the cluster mass function, such as would be detectable observationally only in all-sky surveys. Surprisingly, these objects exhibit a high level of self-similarity, and their dark matter density profiles can be described with the typical NFW profile found in relaxed local systems.

From the Millenium simulations (Fakhouri, Ma & Boylan-Kolchin 2010), high–mass systems with $M > 5 \times 10^{14}\,\mathrm{M}_{\odot}$ at $z = 1$ ($z = 0$) have undergone at least one major merger (mass ratio >1: 3) during the preceding 4 Gyr (12 Gyr). The relaxation time estimated from their crossing time [$t_{\mathrm{cross}} \propto r_{500}/\sigma_{500}$ with $\sigma_{500} = (GM_{500}/r_{500})^{1/2}$] is close to two Hubble times ($t_H = 1/H(z)$), i.e. about 16 Gyr (29 Gyr). A similar conclusion is reached if one
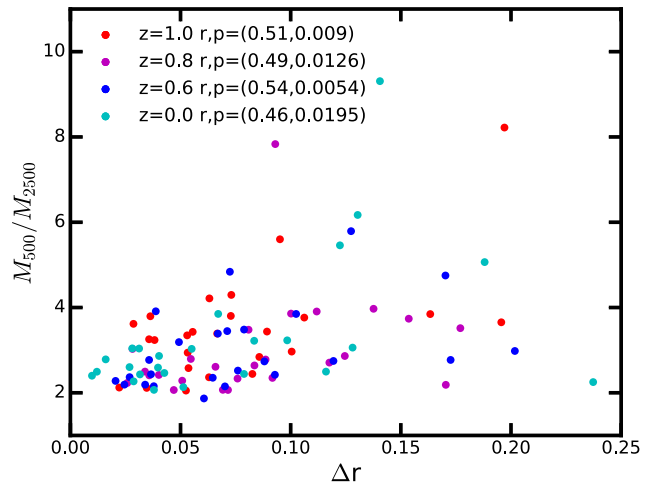
Figure 3. M_{500}/M_{2500} as a function of relaxation state for each redshift slice. The Spearman's rank and the null hypothesis probability are listed in the legend.

uses the dynamical time. We expect that these objects should still be forming and thus be highly unrelaxed. Using Δr as a dynamical indicator, or from visual inspection of the images, we find that the vast majority of the systems in question are indeed unrelaxed.

Naively, one would then expect that the density profiles of such objects would exhibit large variations, linked to the wide variety of dynamical states and formation histories, and that the median profile has not yet converged to the near-universal form of relaxed systems in the local Universe. In contrast, once scaled according to the critical density at each redshift, the density profiles of the clusters in our simulations are remarkably similar, with a low dispersion of less than 0.15 dex within r_{500}. Furthermore, there is little evolution in the radial logarithmic slope or scatter with redshift. This surprising result suggests that the 'universal', 'broken/running' power-law, density profile (e.g. similar to NFW or Einasto) is already in place at $z > 1$ and that it is robust to merging activity. This conclusion is similar to that recently obtained for primordial (Earth–mass) haloes by Angulo et al. (2016) and Ogiya, Nagai & Ishiyama (2016), but at scales that are 21 orders of magnitude larger.

Interestingly, McDonald et al. (2017) recently found a remarkably standard self-similar evolution in the mean profile of the hot gas beyond the cooling core region in massive clusters up to $z \sim 1.9$. This would be a natural consequence of the self-similar evolution of the underlying dark matter distribution that we have shown here, since these systems are dark-matter dominated and the gas evolution, except in the very central regions, is dominated by simple gravitational physics. One could even speculate that McDonald et al.'s finding that the cool core formed early ($z \gtrsim 1.5$) is made possible by the early establishment and stability over time of the centrally cusped dark matter profile. However, the actual demographics of the core properties and their evolution (e.g. the nearly constant cool core mass found by McDonald et al.) will also depend on the specific gas physics (e.g. shocks, cooling, active galactic nucleus feedback).

There is an indication of a residual link between the profile shape and dynamical state, with the most unrelaxed clusters exhibiting a larger dispersion. Future work on a larger sample, covering a wider mass range, will enable us to better characterize both the evolution and the scatter. These are essential to understand the link between profile shape, dynamical state and formation history.

REFERENCES

Angulo R. E., Hahn O., Ludlow A., Bonoli S., 2016, MNRAS, 471, 4687
Bartalucci I., Arnaud M., Pratt G. W., Démoclès J., van der Burg R. F. J., Mazzotta P., 2017, A&A, 598, A61
Bleem L. E. et al., 2015, ApJS, 216, 27
Bleuler A., Teyssier R., Carassou S., Martizzi D., 2015, Comput. Astrophys. Cosmol., 2, 5
Bryan G. L., Norman M. L., 1998, ApJ, 495, 80
Cui W., Borgani S., Murante G., 2014, MNRAS, 441, 1769
Diemer B., Kravtsov A. V., 2014, ApJ, 789, 1
Diemer B., More S., Kravtsov A. V., 2013, ApJ, 766, 25
Fakhouri O., Ma C.-P., Boylan-Kolchin M., 2010, MNRAS, 406, 2267
Gao L., Navarro J. F., Frenk C. S., Jenkins A., Springel V., White S. D. M., 2012, MNRAS, 425, 2169
Hahn O., Abel T., 2011, MNRAS, 415, 2101
Hasselfield M. et al., 2013, J. Cosmol. Astropart. Phys., 7, 008
Hinshaw G. et al., 2013, ApJS, 208, 19
Lewis A., Challinor A., Lasenby A., 2000, ApJ, 538, 473
Martizzi D., Mohammed I., Teyssier R., Moore B., 2014, MNRAS, 440, 2290
McDonald M. et al., 2017, ApJ, 843, 28
Navarro J. F., Frenk C. S., White S. D. M., 1997, ApJ, 490, 493
Navarro J. F. et al., 2004, MNRAS, 349, 1039
Ogiya G., Nagai D., Ishiyama T., 2016, MNRAS, 461, 3385
Peebles P. J. E., 1980, The Large-Scale Structure of the Universe. Princeton Univ. Press, Princeton, NJ
Planck Collaboration XIII, 2016, A&A, 594, A13
Planck Collaboration XVI, 2014, A&A, 571, A16
Planck Collaboration XXIX, 2014, A&A, 571, A29
Planck Collaboration XXVII, 2016, A&A, 594, A27
Power C., Navarro J. F., Jenkins A., Frenk C. S., White S. D. M., Springel V., Stadel J., Quinn T., 2003, MNRAS, 338, 14
Power C., Knebe A., Knollmann S. R., 2012, MNRAS, 419, 1576
Savitzky A., Golay M. J. E., 1964, Anal. Chem., 36, 1627
Schrabback T. et al., 2016, MNRAS, preprint (arXiv:1611.03866)
Tasitsiomi A., Kravtsov A. V., Gottlöber S., Klypin A. A., 2004, ApJ, 607, 125
Teyssier R., 2002, A&A, 385, 337
Velliscig M., van Daalen M. P., Schaye J., McCarthy I. G., Cacciato M., Le Brun A. M. C., Dalla Vecchia C., 2014, MNRAS, 442, 2641
Wu H.-Y., Hahn O., Wechsler R. H., Mao Y.-Y., Behroozi P. S., 2013, ApJ, 763, 70
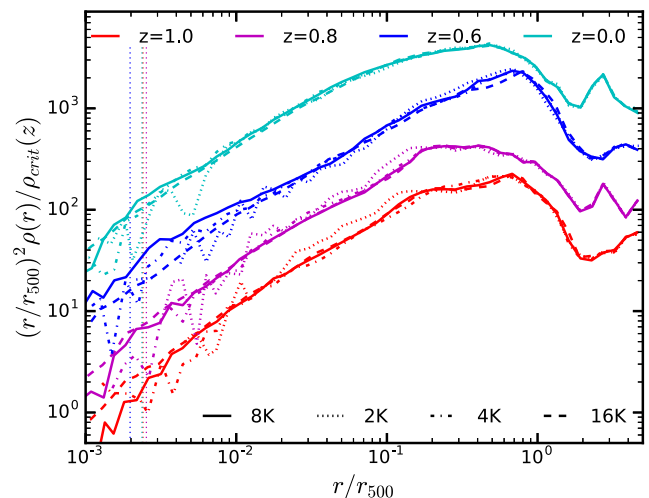
Figure A1. Resolution test for the spherical density profiles for the most massive system of each redshift slice. For clarity, the profiles of the $z_{sel} = 0.8$, 0.6 and 0 systems have been shifted up by a factor of 2, 10 and 20, respectively. The 2 K, 4 K, 8 K (nominal resolution) and 16 K are shown as dotted, dash–dotted, solid and dashed lines, respectively. The resolution limits r_{min} of the 8 K runs are drawn as vertical coloured dotted lines.

APPENDIX A: RESOLUTION STUDY

Fig. A1 shows the results of a resolution study for the most massive system of each redshift slice. The 8 K (i.e. the production runs) and 16 K density profiles are converged over the whole resolved ($r \geq r_{min}^{8K}$) radial range for all the redshift slices. This conclusion applies for all the systems for which resolution tests have been run so far (and not just the most massive system of each redshift slice). As the 2 K and 4 K profiles are significantly different from the 8 K and 16 K over the interesting radial range (i.e. below 10–15 kpc and down to a few kpc that is equivalent to $r/r_{500} \lesssim 1.5 \times 10^{-2}$), an effective resolution of 8192^3 is the minimum required for this work.

This paper has been typeset from a TEX/LATEX file prepared by the author.